A Process Model for the Microstructure Evolution in Ductile Cast Iron: Part I. the Model

M.I. ONSØIEN, Ø. GRONG, Ø. GUNDERSEN, and T. SKALAND

In the present investigation, the multiple phase changes occurring during solidification and subsequent cooling of near-eutectic ductile cast iron have been modeled using the internal state variable approach. According to this formalism, the microstructure evolution is captured mathematically in terms of differential variation of the primary state variables with time for each of the relevant mechanisms. Separate response equations have then been developed to convert the current values of the state variables into equivalent volume fractions of constituent phases utilizing the constraints provided by the phase diagram. The results may conveniently be represented in the form of C curves and process diagrams to illuminate how changes in alloy composition, graphite nucleation potential, and thermal program affect the microstructure evolution at various stages of the process. The model can readily be implemented in a dedicated numerical code for the thermal field in real castings and used as a guiding tool in design of new treatment alloys for ductile cast irons. An illustration of this is given in an accompanying article (Part II).

I. INTRODUCTION

DUCTILE cast irons possess a wide range of physical and mechanical properties, which make them excellent candidate materials for structural applications.[1,2] At the same time, they offer positive impact on economical, safety, and environmental aspects by allowing production of high quality, low priced products from recycled metal scrap. The main disadvantage is weight, but considerable weight savings can be obtained by the use of stronger irons and thinner sections. In practice, this is made possible through a more effective nucleation and growth of the graphite phase during solidification, often in combination with some additional heat treatment of the iron matrix (*e.g.*, austempering).[2]

Because of the increased emphasis on microstructure control, significant progress has been made in the understanding of the mechanisms of microstructure evolution in ductile cast iron over the past decade, both during solidification and in the solid state.[3] At the same time, the recent advances in computer technology and numerical methods have made it possible to analyze transport phenomena (*e.g.*, heat, mass, and fluid flow in the mushy zone) to a high level of detail.[4] A synthesis of that knowledge has, in turn, been consolidated into various kinds of deterministic models to predict the cast structure.[5–13] Some of these also include a consideration of the subsequent solid-state transformations, based on approximate analytical solutions for the carbon diffusion field in the vicinity of the graphite nodules.[6,11] Although the ideal is a true physical model, the approach has shown to work well for certain alloy systems, provided that the models are tuned to experimental microstructure data.

Alternatively, the problem can be handled by means of analytical modeling techniques to ensure a sufficient degree of accuracy in all components of the model without employing complex numerical solutions.[14–18] Experience has shown that constitutive models describing nonisothermal transformation behavior are best derived by using the internal state variable approach, according to the formalism originally proposed by Richmond.[19] In this case, the microstructure evolution is captured mathematically in terms of differential variation of the primary state variables with time for each of the relevant mechanisms.[15,18] At the same time, appropriate heat flow calculations are required to predict the thermal history. Solution of the coupled differential equations is then carried out by stepwise integration in temperature-time space, using an appropriate numerical integration procedure. Moreover, by utilizing the concept of group variables, different kinds of process diagrams and mechanism maps can be constructed to illustrate the competition between the different variables involved.[14–18] In the present investigation, the methodology is further developed and applied to near-eutectic ductile cast irons. Since such irons undergo multiple phase changes during cooling,[1] the real challenge is to couple the different microstructure models in a manner that enforces continuity, compatibility, and equilibrium. The ultimate goal is to establish a complete mathematical relation between the main process variables (*i.e.*, alloy composition, graphite nucleation potential, thermal program, *etc.*) and the end-product microstructure, based on sound physical principles.

Application of the model for construction of process diagrams and optimization of melt treatment practice for some near-eutectic ductile cast irons is described in an accompanying article (Part II).[20]

II. PROBLEM DESCRIPTION

The symbols and units used throughout the article are defined in Appendix I.

A. *General Methodology*

Broadly speaking, a reaction is said to be isokinetic if the increments of transformation behavior in infinitesimal

M.I. ONSØIEN and Ø. GUNDERSEN, Research Metallurgists, are with SINTEF Materials Technology, N-7034 Trondheim, Norway. Ø. GRONG, Professor, is with the Department of Metallurgy, Norwegian University of Science and Technology, N-7034 Trondheim, Norway. T. SKALAND, Research Metallurgist, is with Elkem a/s Research, N-4602 Kristiansand, Norway.

Manuscript submitted March 5, 1997.

isothermal time-steps are additive. Christian[21] defines this mathematically by stating that a reaction is isokinetic if the evolution equation for some state variable X may be written in the form

$$\frac{dX}{dt} = \frac{G(X)}{H(T)} \quad [1]$$

where $G(X)$ and $H(T)$ are arbitrary functions of X and T, respectively.

Equation [1] is a first-order (separable) differential equation, which can be integrated as follows:

$$\int_0^X \frac{dX}{G(X)} = \int_0^t \frac{dt}{H(T)} \quad [2]$$

If the state variable X is a dimensionless parameter, the function $H(T)$ becomes a time constant, which includes the temperature dependence of the reaction. In that case, the right-hand side of Eq. [2] reduces to the well-known Scheil integral.[22]

The internal state variable approach provides a more general formulation of the isokinetic problem. At the simplest level, a microstructure can be described by two state variables, *i.e.*, the volume fraction f and the mean object size r. Alternatively, the number of objects (*e.g.*, particles or grains) per unit volume N may be used in preference to one of these as only two of the variables are independent. During a phase transformation, the microstructure will evolve with time, which, in turn, results in release of heat and a change in T, f, r, or N. Taking f and N as the independent microstructure variables, this change may be described in differential terms as follows:

$$\frac{\partial f}{\partial t} = h_1(f, N, T) \quad [3]$$

$$\frac{\partial N}{\partial t} = h_2(f, N, T) \quad [4]$$

An important feature of the internal state variable approach is that the thermal history is not explicitly built into the models; *i.e.*, the transformation rate depends only on the current values of the state variables. Moreover, if there is no direct coupling between the thermal and microstructure fields, the description of the microstructure evolution reduces to a two or a single state variable problem, depending on the assumptions of the models. In the latter case, it is possible to obtain closed isokinetic solutions, provided that the differential evolution equation contains separable variables of f and T. Otherwise, the solutions will be thermal path dependent, which means that they cannot be generalized to different starting conditions.

B. *Modeling Objectives*

The goal here is not to describe the microstructure evolution in its entirely, but to keep the models as simple as possible without loss of essential ingredients. These two considerations suggest the use of approximate, analytical solutions within the scope of personal computers. Figure 1 shows a schematic representation of the microstructure evolution in near-eutectic ductile cast irons. The important reactions to be modeled are the graphite/austenite eutectic transformation and the ledeburite eutectic transformation during solidification, the subsequent growth of the graphite phase in the austenite regime, and finally, the decomposition of austenite into ferrite and pearlite during the eutectoid transformation. In view of the complexity of the system, the real challenge here is to capture the microstructural connections throughout the entire process route rather than focusing on details of the transformation kinetics within each regime. Thus, for the limiting case of zero nucleation rate ($\partial N/\partial t = 0$), the mathematical treatment of the microstructure evolution reduces to a single state variable problem, which is more easy to handle than the continuous nucleation case in which new graphite nodules form consecutively during solidification. A further reduction in the computational effort can be achieved by assuming that the reactions occur in series (*i.e.*, succession) rather than in parallel, which allows a one-way exchange of inputs and outputs between the different submodels. As shown in Part II,[20] this framework is sufficiently relevant and comprehensive to capture the overall microstructure evolution in ductile cast iron, where the

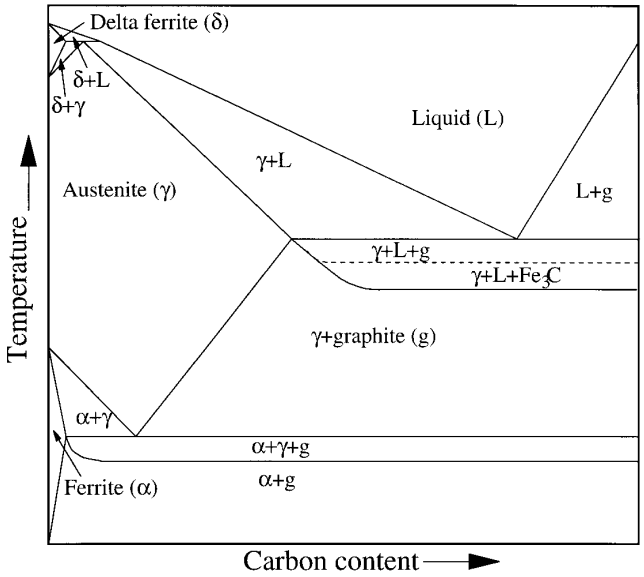

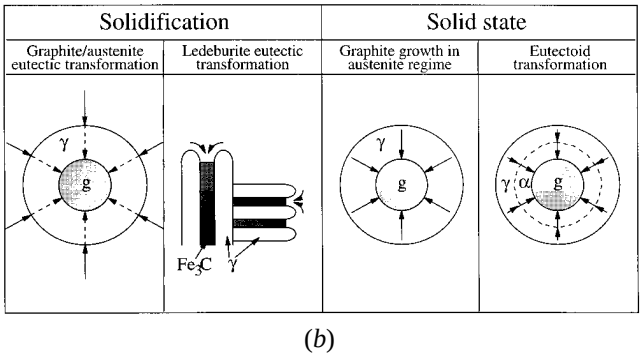

Fig. 1—Schematic representation of the microstructure evolution in near-eutectic ductile cast irons: (a) section of the ternary Fe-C-Si phase diagram and (*b*) close-up of transformation products (arrows indicate direction of carbon diffusion).

graphite formation is stimulated by additions of inoculants to the melt.

C. *Inputs and Outputs of Model*

The primary model inputs will be the initial melt temperature and the alloy composition, from which the fading potential and the equilibrium temperatures for the stable (gray) and metastable (white) eutectics can be evaluated. In addition, information about the nucleation conditions for graphite in the melt is required to illustrate how variations in the inoculation practice affect the microstructure evolution. Since the graphite nucleation temperature $T_{n,s}$ is a measurable quantity,[1,2] it will be regarded as an input parameter in the present process model. Thus, in the numerical simulations, the chosen value of $T_{n,s}$ reflects the potency of the heterogeneous nucleation sites with respect to graphite formation.

The outputs of the model will be the cooling curve and the current microstructural state at a given temperature from which different kinds of process diagrams and mechanism maps can be constructed. Since the response equations converting the fraction transformed into equivalent volume fractions of constituent phases are derived on the basis of constraints provided by the phase diagram, it is also possible to construct a set of "master curves," which show the contribution from each transformation to the total microstructure evolution. This is an attractive aspect of process modeling, because it provides the reader with an overall indication of the microstructural connections throughout the entire process route.

III. MATHEMATICAL MODELING

The present process model consists of several components, *i.e.*, a heat flow model and a series of microstructure models that are coupled.

A. *Heat Flow Model*

For problems involving pure conduction through a liquid, the temperature-time pattern can be calculated by solving the differential heat flow equation for the appropriate boundary conditions:[23]

$$\frac{\partial T}{\partial t} = \frac{1}{\rho c} \nabla[\lambda \nabla T] + \frac{L}{\rho c} \frac{\partial f}{\partial t} \qquad [5]$$

where λ is the thermal conductivity, ρc is the volume heat capacity, L is the latent heat of transformation, and f is the volume fraction of the transformation product.

The form of Eq. [5] implies that the thermal and microstructure fields are fully coupled. In Part II of the investigation,[20] this heat flow equation will be linked to a well-proven experimental casting method (here, directional solidification), which can serve as a model system and provide reliable information about the effect of melt treatment practice on the resulting microstructure evolution. A sketch of the experimental setup is shown in Figure 2. As a starting point, the computational space is divided into a series of interconnected volume elements, each acting as an open system with respect to heat transfer, but being autonomous when it comes to microstructure evolution. The heat flux balance itself is solved using the method of finite differences,

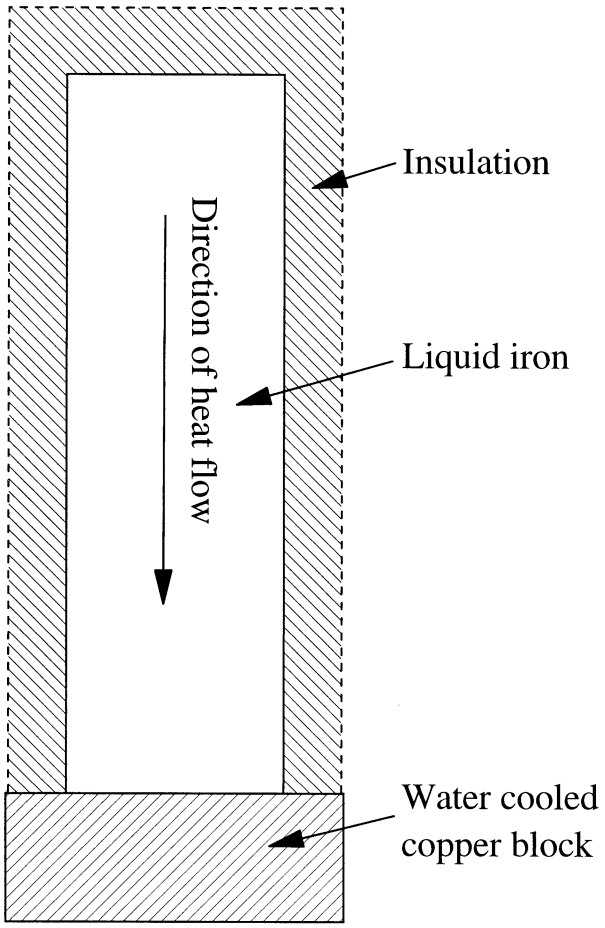

Fig. 2—Principles of directional solidification (schematic).

where a coupled set of ordinary differential equations is derived by integrating Eq. [5] over a representative control volume.

It should be emphasized that the microstructure field can be fully decoupled from Eq. [5] if thermocouple measurements instead are used as a means for obtaining information about the cooling conditions during casting. In that case, the state variable solutions can be used in their closed (isokinetic) form and integrated directly over the actual thermal cycles. This method has been applied in the present investigation to determine the unknown time constants entering the constitutive equations, based on a comparison with experimental microstructure data extracted from the same locations (section IV–A provides further details).

B. *Fading Model*

It is a general observation that the potential for graphite formation during solidification tends to diminish as the time interval between inoculation and casting increases,[2,24] a process frequently referred to as fading. The model adopted here is based on the assumption that nucleation of graphite occurs epitaxially on small (submicroscopic) nonmetallic inclusions, which are entrapped in the liquid after the magnesium treatment and activated by elements supplied through the inoculant.[24] Fading will then occur as a result of a general coarsening of the inclusion population with time. In

the absence of adequate melt stirring, the reaction will be driven by the reduction in the surface energy alone. Under such conditions, the time dependence of the mean inclusion diameter d is given by the Wagner equation:[25]

$$d = (d_0^3 + k_1 t)^{1/3} \quad [6]$$

where d_0 is the inclusion diameter at the time of addition of the inoculant (*i.e.*, when $t = 0$), and k_1 is a kinetic constant.

In the following, we shall assume that Eq. [6] is valid within the entire temperature interval from the initial pouring temperature T_i to $T_{n,s}$, which means that the coarsening process is completed when the graphite nucleation temperature $T_{n,s}$ is reached at time $t = t_{n,s}$.

C. *The Graphite/Austenite Eutectic Transformation*

In general, coupled diffusion problems of the type shown in Figure 1(b) are very complex, and an exact treatment is only possible if Fick's second law is solved numerically in each step for the appropriate boundary conditions. A more pragmatic approach would be to derive the constitutive equations on the basis of approximate analytical solutions that are available in the literature. An example of this is shown in Appendix II, where the classic models of Wetterfall *et al.*[26] and Su *et al.*[27] are used to establish the parabolic growth law. Alternatively, the same evolution equations can be obtained *via* a simplified but stringent one-dimensional (1-D) analysis, where the characteristic spherical geometry of the transformation products is taken into account through a separate set of response equations. This treatment allows coupling of the different submodels in a manner that enforces continuity and equilibrium without a significant increase in the computational effort. At the same time, parabolic kinetics can be implemented in each transformation regime, which follows from the assumption that the subsequent transformations have no memory of the past diffusion fields.

As a starting point, we will first consider isothermal transformation behavior for the limiting case of steady-state diffusion-controlled growth. These solutions will later be manipulated and rewritten in a differential form to cover nonisothermal microstructure evolution, based on the additivity rules advanced by Scheil[22] and Christian.[21] The judicious construction of the constitutive equations makes full use of both dimensionless parameters and calibration techniques to eliminate poorly known kinetic constants. This is essential in order to reduce the total number of variables involved to an acceptable level.

1. *Diffusion model*

The situation is described in Figure 3. According to the assumptions, nucleation of the graphite/austenite constituent starts instantaneously at time $t' = 0$ (*i.e.*, $t = t_{n,s}$) at some point $T = T_{n,s}$ below the stable eutectic temperature $T_{e,s}$. Growth will then proceed without buildup of concentration gradients in the liquid until the metastable eutectic temperature $T_{e,m}$ is reached. In the 1-D analysis, the radius vector r and the temperature T (in a manipulated form) become the primary state variable, which uniquely define the microstructural state during solidification.

Since the graphite/austenite eutectic transformation is a coupled diffusion problem, the carbon flux through both the graphite/austenite interface and the austenite/liquid interface must be considered. In the former case, we may write, using

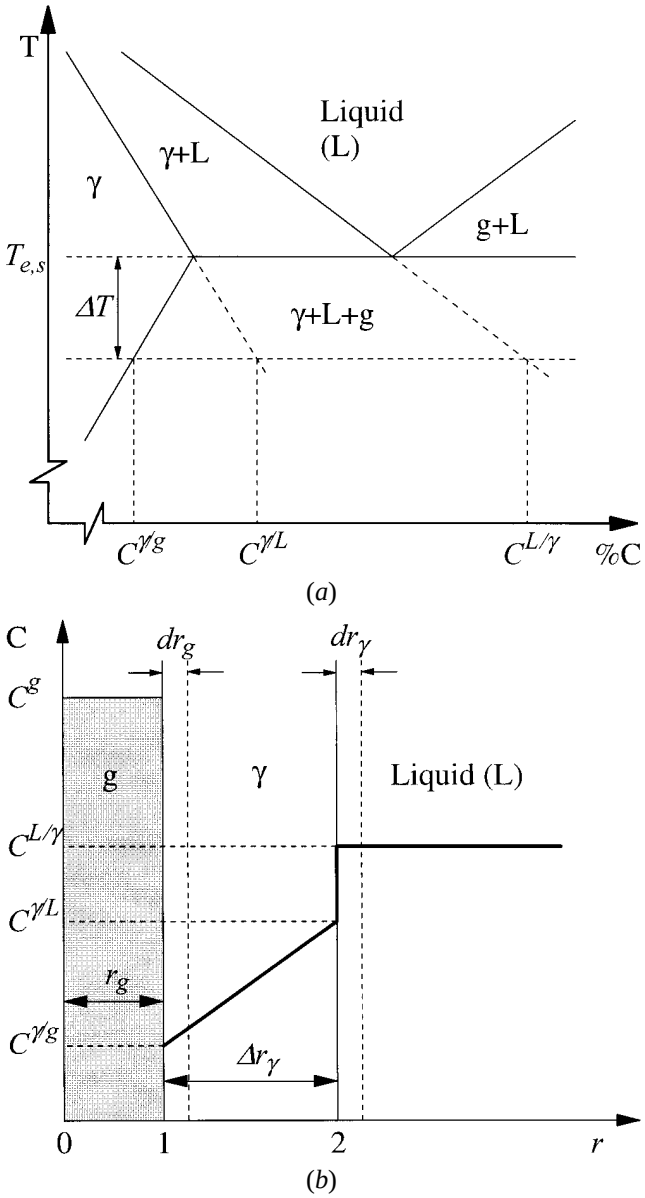

Fig. 3—Simplified diffusion model for the graphite/austenite eutectic transformation: (*a*) sketch of the phase diagram and (*b*) resulting carbon concentration profile across the reaction zone.

Fick's first law and the assumption of a linear carbon concentration profile,

$$(C^g - C^{\gamma/g}) \frac{dr_g}{dt'} = D^\gamma \frac{(C^{\gamma/L} - C^{\gamma/g})}{\Delta r_\gamma} \quad [7]$$

Similarly, the net flux of carbon through the austenite/liquid interface can be written as

$$(C^{L/\gamma} - C^{\gamma/L}) \frac{dr_\gamma}{dt'} = D^\gamma \frac{(C^{\gamma/L} - C^{\gamma/g})}{\Delta r_\gamma} \quad [8]$$

The total thickness of the austenite layer is thus given by

$$\frac{d\Delta r_\gamma}{dt'} = \frac{dr_\gamma}{dt'} - \frac{dr_g}{dt'} \quad [9]$$

from which

$$\frac{d\Delta r_\gamma}{dt'} = M_1 D^\gamma \frac{(C^{\gamma/L} - C^{\gamma/g})}{\Delta r_\gamma} \quad [10]$$

where M_1 is a temperature-dependent concentration factor, defined as

$$M_1 = \left(\frac{C^{\gamma/L} - C^{L/\gamma} + C^g - C^{\gamma/g}}{(C^g - C^{\gamma/g})(C^{L/\gamma} - C^{\gamma/L})}\right) \quad [11]$$

Provided that the temperature remains constant during the transformation, integration of Eq. [10] leads to the following variant of the parabolic growth law:

$$\Delta r_\gamma = \sqrt{2M_1 D^\gamma (C^{\gamma/L} - C^{\gamma/g})(t')} \quad [12]$$

As shown in Appendix II, the form of this equation is similar to that obtained on the basis of a more rigorous analysis, using the classic three-dimensional (3-D) analytical solutions. An exception is the expressions for concentration factors M_1 and M_3, which, of course, are different. Due to the similarity between the two starting equations, the rest of the analysis will be identical as the parameters M_1 and M_3 eventually become embedded in the time constant for the reaction.

By combining Eqs. [7] and [12], it is possible to obtain a relationship between the width of the graphite layer r_g and the corresponding width of the austenite layer Δr_γ. After some manipulation, we arrive at

$$r_g = M_2 \Delta r_\gamma \quad [13]$$

where M_2 is another temperature-dependent (dimensionless) concentration factor, defined as

$$M_2 = \left(\frac{C^{L/\gamma} - C^{\gamma/L}}{C^{\gamma/L} - C^{L/\gamma} + C^g - C^{\gamma/g}}\right) \quad [14]$$

2. *Overall transformation kinetics*

The next step is to develop an isothermal model for the evolution of r_g with time. For the level of detail aimed at here, it is sufficient to regard the graphite/austenite aggregates as compact spheres, which grow at a linear rate defined in the upper limit by Eqs. [12] and [13]. Taking the number of heterogeneous nucleation sites per unit volume of the melt equal to N and the resulting radius of the transformation produces equal to $r_g + \Delta r_\gamma$, the linearized solid fraction Φ' before physical impingement of adjacent transformation volumes becomes

$$\Phi' = (f_s')^{1/3} = \left(\frac{4\pi}{3}\right)^{1/3} (r_g + \Delta r_\gamma)(N)^{1/3} \quad [15]$$

which, after substitution, reads

$$\Phi' = \left(\frac{4\pi}{3}\right)^{1/3} (2M_1 D^\gamma)^{1/2} (C^{\gamma/L} - C^{\gamma/g})^{1/2} \times (t')^{1/2}(1 + M_2)N^{1/3} \quad [16]$$

Consider now a chosen reference alloy containing $N = N_r$ nucleation sites per unit volume, which is subjected to an isothermal quench at a fixed temperature $T = T_{r_1}$ for some time $t' = t_{r_1}$. In this particular case, we may write

$$\Phi_r' = \left(\frac{4\pi}{3}\right)^{1/3} (2M_{1,r} D_r^\gamma)^{1/2} (C_r^{\gamma/L} - C_r^{\gamma/g})^{1/2} \times t_{r_1}^{1/2}(1 + M_{2,r})N_r^{1/3} \quad [17]$$

where index r refers to the experimental conditions defined previously.

Since the eutectic undercooling in the stable system $\Delta T = T_{e,s} - T$ is proportional to the concentration displacement $(C^{\gamma/L} - C^{\gamma/g})$, a combination of Eqs. [16] and [17] gives

$$\Phi' = \Phi_r' \left(\frac{M_1}{M_{1,r}}\right)^{1/2} \left(\frac{D^\gamma}{D_r^\gamma}\right)^{1/2} \left(\frac{\Delta T}{\Delta T_{r_1}}\right)^{1/2} \left(\frac{t'}{t_{r_1}}\right)^{1/2} \left(\frac{1 + M_2}{1 + M_{2,r}}\right) \left(\frac{N}{N_r}\right)^{1/3} \quad [18]$$

Based on Eq. [18], it is possible to define a time constant t_1^* for the system, which takes into account changes in the growth kinetics due to variations in temperature and experimental conditions. The expression for t_1^* is

$$t_1^* = t_{r_1} \left(\frac{M_{1,r}}{M_1}\right) \left(\frac{D_r^\gamma}{D^\gamma}\right) \left(\frac{\Delta T_{r_1}}{\Delta T}\right) \left(\frac{1 + M_{2,r}}{1 + M_2}\right)^2 \left(\frac{N_r}{N}\right)^{2/3} \quad [19]$$

which gives

$$\Phi' = \Phi_r' \left(\frac{t'}{t_1^*}\right)^{1/2} \quad [20]$$

In practice, the temperature dependence of t_1^* is well described by an Arrhenius type of relationship, because the change in the carbon diffusivity with temperature will completely override the corresponding fluctuations in M_1 and M_2, which in this case can be ignored. Thus, by introducing the activation energy for diffusion of carbon in austenite Q^γ in the expression for t_1^*, Eq. [19] becomes

$$t_1^* = t_{r_1} \exp\left[\frac{Q^\gamma}{R}\left(\frac{1}{T} - \frac{1}{T_{r_1}}\right)\right] \left(\frac{\Delta T_{r_1}}{\Delta T}\right) \left(\frac{N_r}{N}\right)^{2/3} \quad [21]$$

In addition, it is necessary to allow for changes in the nucleation conditions in different positions of the casting due to fading. It follows from the previous analysis that fading can be attributed to a general coarsening of the inclusion population with time, which reduces the total number of heterogeneous nucleation sites for graphite in the iron.

Let V_r and V denote the inclusion volume fraction in the reference and the actual alloy, respectively. Since stoichiometric considerations imply that the inclusion volume fraction is proportional to the oxygen and sulfur concentrations in the melt,[24] we may write

$$\frac{V_r}{V} \approx \frac{[\text{wt pct O} + \text{wt pct S}]_r}{[\text{wt pct O} + \text{wt pct S}]} \quad [22]$$

If the total number of heterogeneous nucleation sites for graphite in the iron is taken proportional to the number density of nonmetallic inclusions in the melt at time $t' = 0$ (*i.e.*, $t = t_{n,s}$), we may replace the N_r/N ratio in Eq. [21] by the corresponding $V_r d^3/V d_r^3$ ratio. This leads to the following expression for t_1^*:

$$t_1^* = t_{r_1} \exp\left[\frac{Q^\gamma}{R}\left(\frac{1}{T} - \frac{1}{T_{r_1}}\right)\right]\left(\frac{\Delta T_{r_1}}{\Delta T}\right) \times \left(\frac{[\text{wt pct O} + \text{wt pct S}]_r}{[\text{wt pct O} + \text{wt pct S}]}\right)^{2/3}\left(\frac{d}{d_0}\right)^2 \quad [23]$$

where the input value of d is given by Eq. [6].

The standard Johnson–Mehl correction for physical impingement of adjacent transformation volumes[21] can now be applied to Eq. [20]:

$$\int \frac{d\Phi}{1 - \Phi} = \Phi' \quad [24]$$

which, after integration and some manipulation, yields[17,18]

$$\Phi = f_s^{1/3} = 1 - (1 - \Phi_c)^{(t'/t_1^*)^{1/2}} \quad [25]$$

Equation [25] represents an alternative description of the Avrami equation,[17,18] and is valid as long as the growth rate does not change during the transformation. Therefore, it has the following limiting values and characteristics: $\Phi = 0$ when $t' = 0$, $\Phi = \Phi_c$ when $t' = t_1^*$, and $\Phi \to 1$ when $t' \to \infty$.

3. *Application to continuous cooling*

The modified Avrami equation can readily be applied to nonisothermal transformations by rewriting it in a different form:[17,18]

$$\frac{\partial \Phi}{\partial t'} = \frac{-(1 - \Phi)\ln(1 - \Phi)}{2t_1^*\left[\frac{\ln(1 - \Phi)}{\ln(1 - \Phi_c)}\right]^2} \quad [26]$$

Equation [26] is a first-order separable differential equation, which satisfies the additivity conditions pertaining to an isokinetic reaction.[21] Because the transformation rate in this case depends only on the current values of the state variables r and T (here, represented by Φ and t_1^*, respectively), it can be readily coupled with Eq. [5] and solved numerically, taking $f = f_s = \Phi^3$ and $L = L_s$ in the heat flow model.

4. *Response equations*

Due to the assumption of a planar interface configuration in the derivation of the rate law, Eq. [13] cannot readily be applied to predict the individual volume fractions of graphite and austenite after solidification in the case of a spherical geometry. More refined calculations suggest that the ratio between the radius of the graphite sphere r_g and the corresponding radius of the entire graphite/austenite nodule $r_g + \Delta r_\gamma$ should be close to 2.4.[27] This gives a maximum (equilibrium) volume fraction of graphite f_{eq}^o of $(1/2.4)^3 \approx 0.072$. A slightly higher volume fraction is obtained from the Fe-C phase diagram at 2.5 wt pct Si, using the lever rule and reasonable average values for the graphite and iron densities (*i.e.*, $\rho_g = 2000$ and $\rho_{Fe} = 7300$ kg m^{-3}). For a typical carbon content of 3.5 wt pct, f_{eq}^o is close to 0.083 at $T = T_{e,m}$. If the same analysis is applied to an incomplete transformation (*i.e.*, $f_s < 1$), we may write

$$f_g^o = f_{eq}^o f_s = f_{eq}^o \Phi^3 \quad [27]$$

$$f_\gamma^o = (1 - f_{eq}^o) f_s = (1 - f_{eq}^o)\Phi^3 \quad [28]$$

$$f_{lb}^o = 1 - f_g^o - f_\gamma^o = 1 - f_s = 1 - \Phi^3 \quad [29]$$

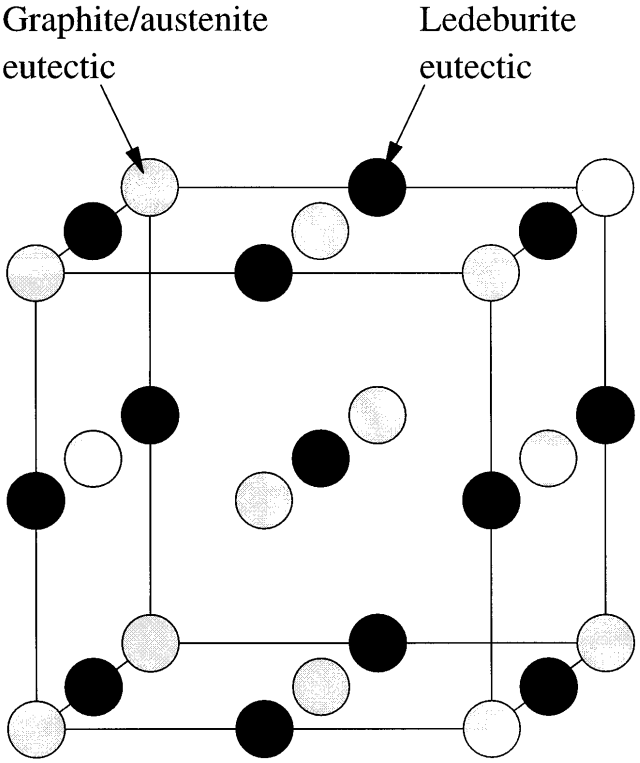

Fig. 4—Assumed spatial distribution of eutectic phases in iron matrix.

where f_g^o, f_γ^o, and f_{lb}^o refer to the individual volume fractions of graphite, austenite, and ledeburite, respectively, in the solidified iron.

According to this model, the output is fixed when the metastable eutectic temperature is reached at $T = T_{e,m}$. Hence, solidification below that temperature will not change the numerical values of the calculated volume fractions.

D. *The Ledeburite Eutectic Transformation*

The assumption that the different reactions occur in succession is convenient from a modeling point of view, because it simplifies the subsequent analysis of the ledeburite eutectic transformation.

1. *Isothermal microstructure model*

If the graphite/austenite nodule distribution is approximated by that of a close-packed face-centered space lattice, the ledeburite eutectic will appear in intermediate positions, as shown in Figure 4. This means that the total number of sites available for nucleation per unit volume is essentially the same as the number density of graphite/austenite nodules in the melt. The next step is to adopt a spherical grain morphology and invoke the simplifying assumption that nucleation occurs instantaneously at time $t'' = 0$ (*i.e.*, $t = t_{n,m}$) at some point $T = T_{n,m}$ below the metastable eutectic temperature $T_{e,m}$. Taking the radius of the nodules equal to r_{lb}, the linearized volume fraction of ledeburite X' become

$$X' = \left(\frac{f'_{lb}}{f_{lb}^o}\right)^{1/3} = \left(\frac{4\pi}{3}\right)^{1/3} r_{lb}(N)^{1/3}\left(\frac{1}{f_{lb}^o}\right)^{1/3} \quad [30]$$

At a fixed temperature below the metastable eutectic temperature, the growth velocity of the nodules v will be proportional to the square of the bulk undercooling $\Delta T^* = T_{e,m} - T$;[8,28] *i.e.*, $r_{lb} = vt'' = k_2(\Delta T^*)^2 t''$, which gives

$$X' = \left(\frac{4\pi}{3}\right)^{1/3} k_2(\Delta T^*)^2 t''(N)^{1/3}\left(\frac{1}{f^o_{lb}}\right)^{1/3} \quad [31]$$

If the same analysis is carried out for the reference alloy (characterized by $T = T_{r_1}$, $t'' = t_{r_2}$, $\Delta T^* = \Delta T^*_{r_2}$, $N = N_r$, and $f^o_{lb} = 1$), we obtain

$$X'_r = \left(\frac{4\pi}{3}\right)^{1/3} k_2(\Delta T^*_{r_2})^2 t''_{r_2}(N_r)^{1/3} \quad [32]$$

A combination of Eqs. [31] and [32] then gives

$$X' = X'_r\left(\frac{\Delta T^*}{\Delta T^*_{r_2}}\right)^2\left(\frac{t''}{t_{r_2}}\right)\left(\frac{N}{N_r}\right)^{1/3}\left(\frac{1}{f^o_{lb}}\right)^{1/3} \quad [33]$$

We may now introduce the time constant t^*_2 for the system, defined as

$$t^*_2 = t_{r_2}\left(\frac{\Delta T^*_{r_2}}{\Delta T^*}\right)^2\left(\frac{N_r}{N}\right)^{1/3}(f^o_{lb})^{1/3} \quad [34]$$

After substitution, Eq. [34] reads

$$t^*_2 = t_{r_2}\left(\frac{\Delta T^*_{r_2}}{\Delta T^*}\right)^2\left(\frac{[\text{wt pct O} + \text{wt pct S}]_r}{[\text{wt pct O} + \text{wt pct S}]}\right)^{1/3}\left(\frac{d}{d_0}\right)(f^o_{lb})^{1/3} \quad [35]$$

from which

$$X' = X'_r\left(\frac{t''}{t^*_2}\right) \quad [36]$$

where the input value of d is given by Eq. [6].

The standard Johnson–Mehl correction for physical impingement of adjacent transformation volumes[21] can now be applied to Eq. [36]:

$$\int \frac{dX}{1 - X} = X' \quad [37]$$

which, after integration and some manipulation, yields[17,18]

$$X = \left(\frac{f_{lb}}{f^o_{lb}}\right)^{1/3} = 1 - (1 - X_c)^{(t''/t^*_2)} \quad [38]$$

2. *Application to continuous cooling*

As in the previous case, the modified Avrami equation can readily be applied to nonisothermal transformations by rewriting it in a differential form:[17,18]

$$\frac{\partial X}{\partial t''} = -\frac{(1 - X)\ln(1 - X)}{t^*_2\left[\frac{\ln(1 - X)}{\ln(1 - X_c)}\right]} \quad [39]$$

Equation [39] can be coupled with Eq. [5] and solved numerically by stepwise integration in temperature-time space, taking $f = f_{lb} = f^o_{lb}X^3$ and $L = L_m$ in the heat flow model.

E. *Graphite Growth in Austenite Regime*

The next problem to consider is growth of the graphite phase in the austenite regime. As shown by the schematic phase diagram in Figure 1(a), the driving force for this reaction is provided by the decrease in the carbon solid solubility with temperature. For near-eutectic ductile cast irons, the corresponding change in the equilibrium volume fraction of graphite f_{eq} with temperature (in Kelvin) can be expressed as

$$f_{eq} = \frac{(\text{pct C} + 1.1 - 0.0016T)(\rho_{\text{Fe}}/\rho_g(100 - \text{pct C}))}{1 + (\text{pct C} + 1.1 - 0.0016T)(\rho_{\text{Fe}}/\rho_{\text{g}}(100 - \text{pct C}))} \quad [40]$$

It follows that f_{eq} increases from about 0.083 at the eutectic temperature to approximately 0.10 at the eutectoid temperature T_{ed} (in the model, these limiting values are referred to as f^o_{eq} and f^*_{eq}, respectively).

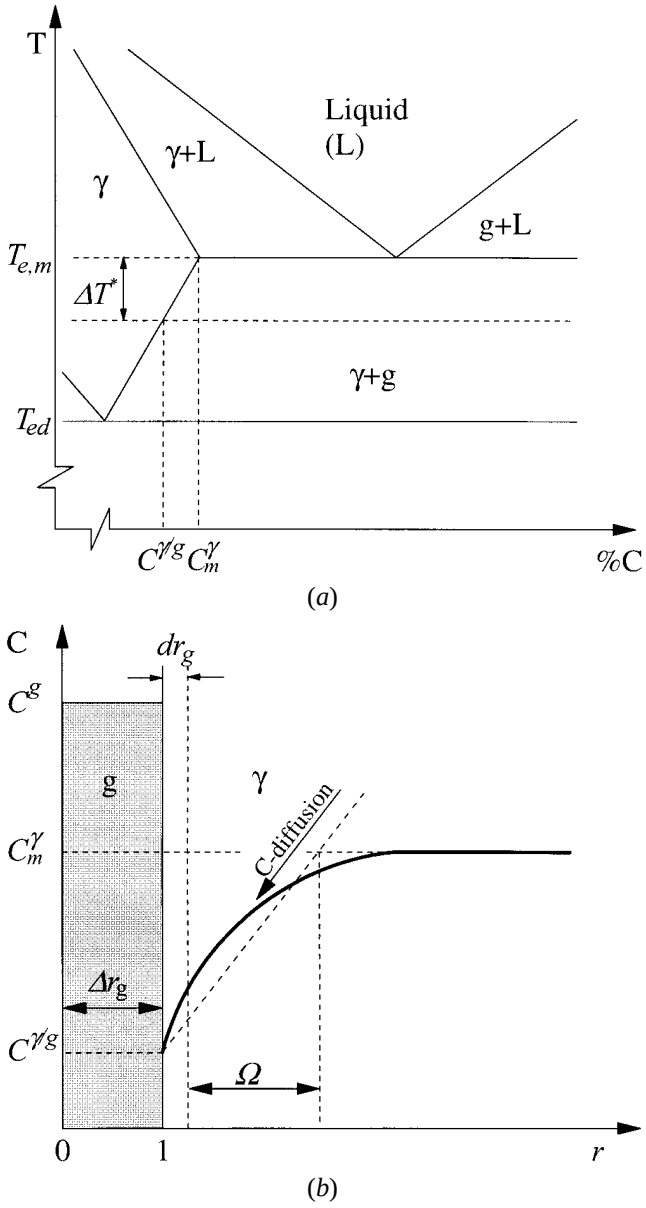

Fig. 5—Simplified diffusion model for graphite growth in the austenite regime: (*a*) sketch of the phase diagram and (*b*) resulting carbon concentration profile across the reaction zone.

1. *Diffusion model*

As in the previous cases, the growth kinetics are derived on the basis of a simple 1-D diffusion model. Referring to Figure 5, growth of the graphite phase occurs by diffusion of carbon from the austenite to the γ/g interface. The reaction starts at time $t'' = 0$ (*i.e.*, $t = t_{n,m}$) when the graphite/austenite

eutectic transformation is completed. By using Fick's first law and the assumption of a linear carbon concentration profile, the displacement of the γ/g interface can be expressed as

$$(C^g - C^{\gamma/g})\frac{dr_g}{dt''} = D^\gamma \frac{(C_m^\gamma - C^{\gamma/g})}{\Omega} \quad [41]$$

where C_m^γ is the initial carbon content in the austenite matrix (here, taken equal to the equilibrium value at $T = T_{e,m}$), and Ω is the corresponding width of the diffusion zone.

Moreover, conservation of matter implies that

$$\Omega \approx \frac{2(C^g - C_m^\gamma)\Delta r_g}{(C_m^\gamma - C^{\gamma/g})} \quad [42]$$

A combination of Eqs. [41] and [42] then gives

$$\frac{dr_g}{dt''} = \frac{D^\gamma (C_m^\gamma - C^{\gamma/g})^2}{2(C^g - C^{\gamma/g})(C^g - C_m^\gamma)\Delta r_g} \quad [43]$$

Assuming isothermal conditions, integration of Eq. [43] leads to the following variant of the parabolic growth law:

$$\Delta r_g = \sqrt{D^\gamma K t''} \quad [44]$$

where K is a dimensionless concentration factor, defined as

$$K = \frac{(C_m^\gamma - C^{\gamma/g})^2}{(C^g - C^{\gamma/g})(C^g - C_m^\gamma)} \quad [45]$$

2. *Overall transformation kinetics*

Rejection of carbon from the austenite during cooling results in an increase in the graphite volume fraction. During the early stages of the process (before impingement of neighboring diffusion fields occurs), this change can be expressed as

$$(f_g')^{1/3} = \left(\frac{4\pi}{3}\right)^{1/3} (r_g^o + \Delta r_g)(N)^{1/3} \quad [46]$$

where r_g^o is the radius of the graphite sphere at time $t'' = 0$.

The radius r_g^o is, in turn, given as

$$r_g^o = \left(\frac{4\pi}{3}\right)^{-1/3} (f_g^o)^{1/3}(N)^{-1/3} \quad [47]$$

A combination of Eqs. [44], [46], and [47] then gives

$$\Delta r_g = \left(\frac{4\pi}{3}\right)^{-1/3} (N)^{-1/3}[(f_g')^{1/3} - (f_g^o)^{1/3}] = \sqrt{D^\gamma K t''} \quad [48]$$

from which

$$(f_g')^{1/3} - (f_g^o)^{1/3} = \left(\frac{4\pi}{3}\right)^{1/3} (D^\gamma)^{1/2}(K)^{1/2}(t'')^{1/2}(N)^{1/3} \quad [49]$$

In order to arrive at a solution that satisfies the constraints provided by the phase diagram, we introduce the parameter Y', defined as

$$Y' = \frac{(f_g')^{1/3} - (f_g^o)^{1/3}}{(f_s f_{eq})^{1/3} - (f_g^o)^{1/3}} = \left(\frac{4\pi}{3}\right)^{1/3} (D^\gamma)^{1/2}(K)^{1/2}(t'')^{1/2}(N)^{1/3}\left(\frac{1}{(f_s f_{eq})^{1/3} - (f_g^o)^{1/3}}\right) \quad [50]$$

The next step is to invoke the reference alloy (characterized by $T = T_{r_3}$, $t'' = t_{r_3}$, $N = N_r$, and $f_s = 1$):

$$Y_r' = \left(\frac{4\pi}{3}\right)^{1/3} (D_r^\gamma)^{1/2}(K_r)^{1/2}(t_{r_3})^{1/2}(N_r)^{1/3} \times \left(\frac{1}{(f_{eq,r})^{1/3} - (f_{eq}^o)^{1/3}}\right) \quad [51]$$

A combination of Eqs. [50] and [51] gives

$$Y' = Y_r'\left(\frac{D^\gamma}{D_r^\gamma}\right)^{1/2}\left(\frac{K}{K_r}\right)^{1/2}\left(\frac{N}{N_r}\right)^{1/3} \times \left(\frac{t''}{t_{r_3}}\right)^{1/2} \frac{(f_{eq,r})^{1/3} - (f_{eq}^o)^{1/3}}{(f_s f_{eq})^{1/3} - (f_g^o)^{1/3}} \quad [52]$$

After substituting for D^γ and N/N_r in Eq. [52], the time constant t_3^* for the system becomes

$$t_3^* = t_{r_3}\left(\frac{K_r}{K}\right)\exp\left[\frac{Q^\gamma}{R}\left(\frac{1}{T} - \frac{1}{T_{r_3}}\right)\right] \times \left(\frac{[\text{wt pct O} + \text{wt pct S}]_r}{[\text{wt pct O} + \text{wt \% S}]}\right)^{2/3}\left(\frac{d}{d_0}\right)^2 \times \left[\frac{(f_s f_{eq})^{1/3} - (f_g^o)^{1/3}}{(f_{eq,r})^{1/3} - (f_{eq}^o)^{1/3}}\right]^2 \quad [53]$$

from which

$$Y' = Y_r'\left(\frac{t''}{t_3^*}\right)^{1/2} \quad [54]$$

where the input value of d is given by Eq. [6].

After correcting for physical impingement of adjacent transformation volumes, we obtain

$$Y = \frac{(f_g)^{1/3} - (f_g^o)^{1/3}}{(f_s f_{eq})^{1/3} - (f_g^o)^{1/3}} = 1 - (1 - Y_c)^{(t''/t_3^*)^{1/2}} \quad [55]$$

3. *Application to continuous cooling*

As in the previous cases, the modified Avrami equation can be applied to a nonisothermal situation by rewriting it in a differential form:[17,18]

$$\frac{\partial Y}{\partial t''} = \frac{-(1 - Y)\ln(1 - Y)}{2t_3^*\left[\frac{\ln(1 - Y)}{\ln(1 - Y_c)}\right]^2} \quad [56]$$

Since the evolution parameter Y depends on temperature (*i.e.*, f_{eq}), Eq. [56] is a nonseparable differential equation, which must be solved using an appropriate numerical integration procedure. However, because there is no release of transformation heat in the austenite regime, the thermal program is not influenced by the microstructure evolution as assumed in the previous cases.

4. *Response equations*

By utilizing the constraints provided by the phase diagram, it is possible to derive a set of self-consistent response equations, which yield the resulting volume fractions of graphite, austenite, and ledeburite at the entry of the eutectoid transformation (*i.e.*, when $f_g = f_g^*$ and $f_{eq} = f_{eq}^*$):

$$f_g^* = f_s[Y((f_{eq}^*)^{1/3} - (f_{eq}^o)^{1/3}) + (f_{eq}^o)^{1/3}]^3 \quad [57]$$

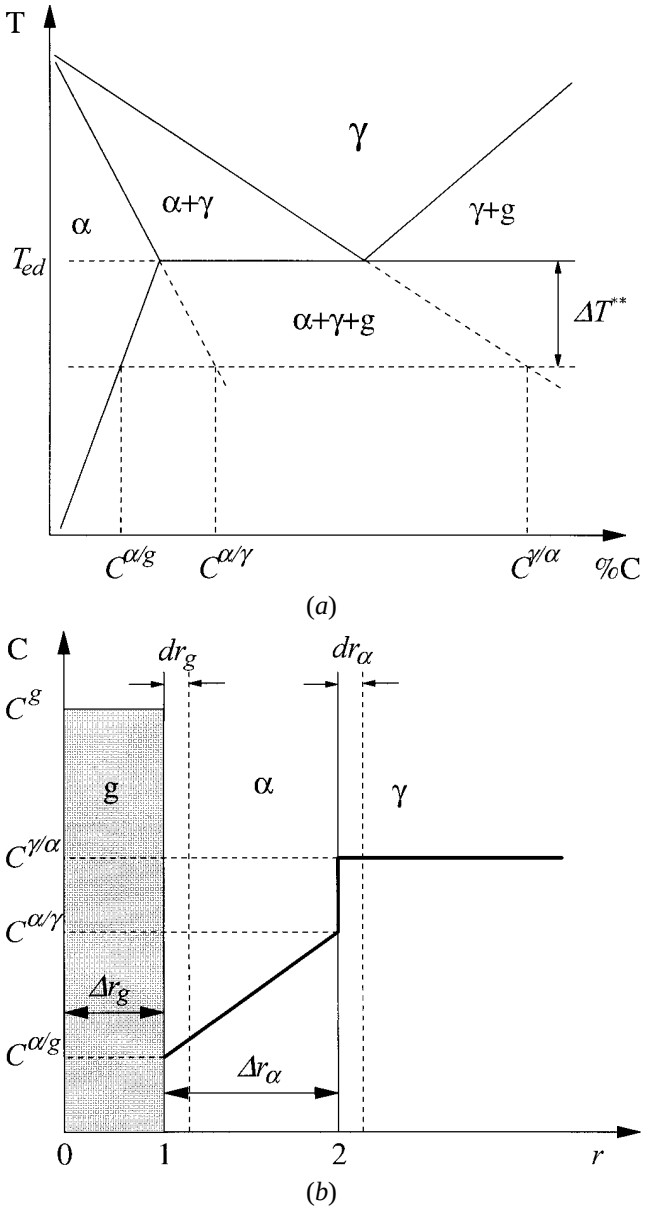

Fig. 6—Simplified diffusion model for the eutectoid transformation: (*a*) sketch of the phase diagram and (*b*) resulting carbon concentration profile across the reaction zone.

$$f_\gamma^* = f_s - f_g^* \quad [58]$$

$$f_{lb}^* = 1 - f_s \quad [59]$$

These relations are based on the assumption that the ledeburite eutectic does not decompose into graphite and austenite during cooling down to the eutectoid temperature.

F. *The Eutectoid Transformation*

The last reaction to consider is the eutectoid transformation. Figure 6 shows a sketch of the model system adopted in the present investigation.

1. *Microstructure model*

According to the assumptions, the graphite nodules are surrounded by an outer shell of ferrite, which starts to grow at time $t''' = 0$ (*i.e.*, $t = t_{ed}$) when the eutectoid temperature T_{ed} is reached. Provided that there are no concentration gradients within the asutenite, growth of the graphite phase will occur at a rate that is controlled by diffusion of carbon through the ferrite. Because this model is essentially the same as the one shown in Figure 3 for growth of graphite/austenite during the eutectic transformation, the mathematical treatment (and thus the governing evolution equations) will be similar in both cases. Accordingly, under isothermal heat treatment conditions, the width of the ferrite layer Δr_α is given by

$$\Delta r_\alpha = \sqrt{2M_1^* D^\alpha (C^{\alpha/\gamma} - C^{\alpha/g})(t''')} \quad [60]$$

where M_1^* is a temperature-dependent concentration factor, defined as

$$M_1^* = \left(\frac{C^{\alpha/\gamma} - C^{\gamma/\alpha} + C^g - C^{\alpha/g}}{(C^g - C^{\alpha/g})(C^{\gamma/\alpha} - C^{\alpha/\gamma})} \right) \quad [61]$$

Similarly, the increase in the radius of the graphite nodules can be written as

$$\Delta r_g = M_2^* \Delta r_\alpha \quad [62]$$

where M_2^* is another temperature-dependent (dimensionless) concentration factor, defined as

$$M_2^* = \left(\frac{C^{\gamma/\alpha} - C^{\alpha/\gamma}}{C^{\alpha/\gamma} - C^{\gamma/\alpha} + C^g - C^{\alpha/g}} \right) \quad [63]$$

2. *Overall transformation kinetics*

Because the solubility of carbon in ferrite is very small, it is a reasonable approximation to neglect the variation in the equilibrium carbon concentration with temperature and instead use a constant value for the volume of graphite in the two-phase regime (in the following designated f_{eq}^{**}). Under such conditions, the evolution equation becomes

$$Z = \frac{(f_g^{**})^{1/3} - (f_g^*)^{1/3}}{(f_s f_{eq}^{**})^{1/3} - (f_g^*)^{1/3}} = 1 - (1 - Z_c)^{(t'''/t_4^*)^{1/2}} \quad [64]$$

where the time constant t_4^* is given by the following expression:

$$t_4^* = t_{r_4} \exp\left[\frac{Q^\alpha}{R} \left(\frac{1}{T} - \frac{1}{T_{r_4}} \right) \right] \left(\frac{\Delta T_{r_4}^{**}}{\Delta T^{**}} \right) \times \left(\frac{[\text{wt pct O} + \text{wt pct S}]_r}{[\text{wt pct O} + \text{wt pct S}]} \right)^{2/3} \left(\frac{d}{d_0} \right)^2 \times \left(\frac{(f_s f_{eq}^{**})^{1/3} - (f_g^*)^{1/3}}{(f_{eq}^{**})^{1/3} - (f_{eq}^*)^{1/3}} \right)^2 \quad [65]$$

Note that the temperature dependence of the concentration factors is ignored in the derivation of Eq. [65].

3. *Application to continuous cooling*

By analogy, the nonisothermal case is dealt with by rewriting Eq. [64] in a differential form:

$$\frac{\partial Z}{\partial t'''} = \frac{-(1 - Z) \ln (1 - Z)}{2t_4^* \left[\frac{\ln (1 - Z)}{\ln (1 - Z_c)} \right]^2} \quad [66]$$

Solution of the coupled differential Eqs. [5] and [66] is then carried out by stepwise integration in temperature-time

Table I. Chemical Composition of Reference Iron (in Weight Percent)

Element	C	Si	Mn	P	Mg	Ti	Al	Pb
Value	3.51	2.13	<0.03	0.025	0.042	0.016	0.014	<0.006

space, taking $f = f_\alpha$ (the volume fraction of ferrite) and $L = L_e$ in the heat flow model.

4. *Response equations*

During the eutectoid transformation, the austenite decomposes into graphite and ferrite (α). Normally, the reaction will be incomplete (*i.e.*, $Z < 1$), which means that the remaining fraction transforms to pearlite (p). At the same time, the ledeburite phase becomes trapped in the form of carbide/ferrite aggregates (cf). Since a full mathematical description of the microstructure evolution would require separate treatments of all four reactions, a more pragmatic approach is adopted here, based on the assumption that there is no coupling between the different transformations. In the present context, this means that the phase relations are fixed when the primary eutectoid reaction is completed:

$$f_g^{**} = [Z((f_s f_{eq}^{**})^{1/3} - (f_g^*)^{1/3}) + (f_g^*)^{1/3}]^3 \quad [67]$$

$$f_\alpha = (f_s - f_g^{**})\left[\frac{f_g^{**} - f_g^*}{f_s f_{eq}^{**} - f_g^*}\right] \quad [68]$$

$$f_p = f_s - f_g^{**} - f_\alpha \quad [69]$$

$$f_{cf} \approx f_{lb}^* = f_{lb}^o = 1 - f_s \quad [70]$$

Note that the contribution from previous transformations is also implicitly built into these response equations through the parameters f_g^* and f_s.

IV. ANALYSIS OF THE MODEL

Several important points can be deduced from the process model without solving the differential evolution equations, provided that the required input data are available. Most of the data can be obtained from well-established sources, but some must also be acquired by tuning the models to experimental microstructure data. The latter method is used to determine the reference times (*i.e.*, time constants) in the temperature-dependent functions entering the modified Avrami equation.

A. *Calibration Procedure*

The reference iron included in the investigation is produced from high purity pig iron, using a conventional magnesium-containing FeSi treatment alloy and inoculant. Directional solidification is carried out by pouring the superheated liquid metal into a 40-mm-diameter and 140-mm-long insulated mold made of aluminosilicate fibers, which is cooled from the bottom by means of a water-cooled copper chill. Thermocouples are then placed at fixed positions from the chilled end to register the temperature-time pattern during cooling. Details of the experimental procedure have been reported elsewhere.[29] Tables I and II contain a summary of chemical composition and microstructure data.

Figure 7 shows a sketch of the longitudinal section of the bar. Three different zones are indicated, *i.e.*, the chill zone (~100 pct iron carbide), the transition zone, and the iron carbide free zone. The temperature and microstructure data recorded for transition zone provide a basis for calibrating the solidification models. Similarly, data from the carbide free zone can be used to determine the time constant for eutectoid transformation. In practice, this is done by integrating the evolution equations over the measured cooling curve for chosen values of t_{r_1} and t_{r_2} until a good agreement between theory and experiments is obtained. Because the input data for the thermal program are acquired from measurements, the integration can be carried out using the more convenient isokinetic solutions:[17,18]

Table II. Microstructure Data Used for Calibration of Unknown Kinetic Constants in Avrami Equation

Position Referred to Chilled End of Bar, l (mm)	Fraction of Austenite/ Graphite Eutectic, f_s	Fraction of Ledeburite Eutectic, $1 - f_s$	Nodule Count, N_r (no. mm^{-3})*
15	~0.94	~0.06	12696
35	1	0	8731

*Estimated from two-dimensional microstructure data.

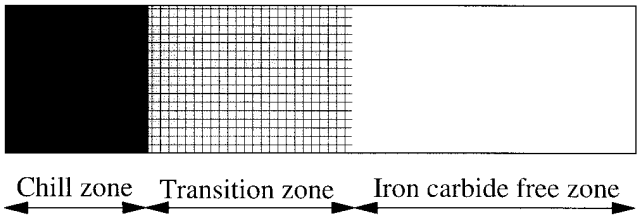

Fig. 7—Schematic diagram showing the change in solidification microstructure with position from chilled end of bar.

$$\Phi = f_s^{1/3} = 1 - (1 - \Phi_c)^{(\int_0^{t'} dt'/t_1^*)^{1/2}} \quad [71]$$

$$X = \left(\frac{f_{lb}}{f_{lb}^o}\right)^{1/3} = 1 - (1 - X_c)^{(\int_0^{t''} dt''/t_2^*)} \quad [72]$$

and

$$Z = \frac{(f_g^{**})^{1/3} - (f_g^*)^{1/3}}{(f_s f_{eq}^{**})^{1/3} - (f_g^*)^{1/3}} = 1 - (1 - Z_c)^{(\int_0^{t'''} dt'''/t_4^*)^{1/2}} \quad [73]$$

These solutions contain the well-known Scheil integral,[22] which simply is a measure of the kinetic strength of the cooling cycle with respect to microstructure evolution.

Similarly, the time constant in the diffusion model for graphite growth in the austenite regime can be evaluated from Eq. [50], using experimental data for the graphite nodule density N_r in the carbide free zone. The appropriate expression for t_{r_3} is

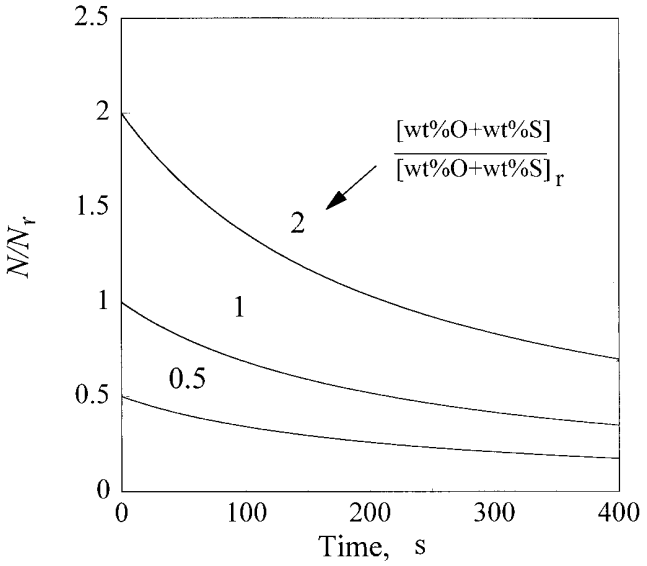

Fig. 8—Predicted fading curves for near-eutectic ductile cast iron showing the relative change in the nodule count with retention time in the liquid state for different starting conditions. Input data as in Table III.

$$t_{r_3} = (Y_c)^2\left(\frac{3}{4\pi}\right)^{2/3}(f_{eq,r}^{1/3} - f_{eq}^{o1/3})^2\left(\frac{1}{D_r^\gamma}\right) \times \left(\frac{1}{K_r}\right)\left(\frac{1}{N_r}\right)^{2/3}\left(\frac{d_0}{d}\right)^2 \quad [74]$$

Table III contains a summary of all input data used in the present modeling exercise.

B. *Conditions for Graphite Nucleation during Solidification*

From a kinetic point of view, nucleation of graphite during solidification can either be regarded as an instantaneous or a continuous process. In the former case, fading can be modeled by considering the stability of the heterogeneous nucleation sites in the melt prior to solidification (*i.e.*, the change in the number density with time). The simple coarsening model adopted here predicts that the graphite nodule density N should fall from its initial value N_r according to the following relationship:

$$\frac{N}{N_r} = \frac{Vd_o^3}{V_r d^3} = \frac{[\text{wt pct O} + \text{wt pct S}]}{[\text{wt pct O} + \text{wt pct S}]_r}\left(\frac{d_o^3}{d_o^3 + k_1 t}\right) \quad [75]$$

Figure 8 shows a graphical representation of Eq. [75] for different starting conditions, using input data from Table III. It is evident that the expected decay in the nucleation potential with time is readily captured by the model.[24] During directional solidification, this will lead to a decrease in the graphite nodule density with increasing distance from the cooled end of the bar, in agreement with experimental observations. If graphite nucleation instead is regarded as a continuous process following the treatment of Skaland *et al.*,[24] the pattern observed in Figure 8 is not significantly changed. Hence, the simplifying assumption of early site saturation is not critical in the sense that it alters the outcome of the analysis.

Table III. Summary of Input Data Used in Microstructure Models

Parameter	Value	Comments
d_0	1.33 μm	obtained from data reported by Skaland *et al.*[23]
k_1	0.011 $\mu m^3\ s^{-1}$	
$T_{e,s}$	1162.5 °C	calculated from bulk composition using appropriate formula*[30]
$T_{n,s}$	1160 °C	chosen
T_{r_1}	1158 °C	fixed
Q^γ	134 kJ mol^{-1}	activation energy for diffusion of C in austenite[31]
t_{r_1}	0.02 s	obtained by calibration to experimental microstructure data
Φ_c	0.05	fixed
$T_{e,m}$	1116.1 °C	calculated from bulk composition using appropriate formula**[30]
$T_{n,m}$	1116 °C	chosen
T_{r_2}	1115 °C	fixed
t_{r_2}	100 s	obtained by calibration to experimental microstructure data
X_c	0.05	fixed
T_{ed}	771.8 °C	calculated from bulk composition using appropriate formula†[30]
T_{r_3}	1000 °C	fixed
D_r (at T_{r_3})	$4.4 \times 10^{-11}\ m^2\ s^{-1}$	calculated from data reported in Ref. 31
K_r (at T_{r_3})	1×10^{-4}	calculated
N_r	8731 no. mm^{-3}	obtained from measurements (Table II)
t_{r_3}	0.041 s	calculated
Y_c	0.05	fixed
Q^α	87 kJ mol^{-1}	activation energy for diffusion of C in ferrite[31]
T_{r_4}	760 °C	fixed
t_{r_4}	4.5 s	obtained by calibration to experimental microstructure data
Z_c	0.05	fixed
ρ_g	2000 kg m^{-3}	chosen
ρ_{Fe}	7300 kg m^{-3}	chosen
f_{eq}^o	0.083	calculated from the Fe-C diagram at 2.5 wt pct Si using the lever rule
f_{eq}^*	0.100	
f_{eq}^{**}	0.117	

*$T_{e,s}$ (°C) = 1154 + 4 pct Si − 2 pct Mn.
**$T_{e,m}$ (°C) = 1148 − 15 pct Si + 3 pct Mn.
†T_{ed} (°C) = 740 + 15 pct Si − 3.5 pct Mn.

C. *Construction of C Curves*

An attractive feature of the present modeling approach is that it allows the construction of various kinds of process diagrams such as C curves or continuous cooling transformation diagrams. Examples of the former type are given in Figure 9, using Eqs. [23], [35], [53], and [65] and input data from Table III.

It is evident from Figures 9(a) and (d) that both the graphite/austenite eutectic transformation and the eutectoid transformation are characterized by true C curves due to the competitive influence of driving force (undercooling ΔT)

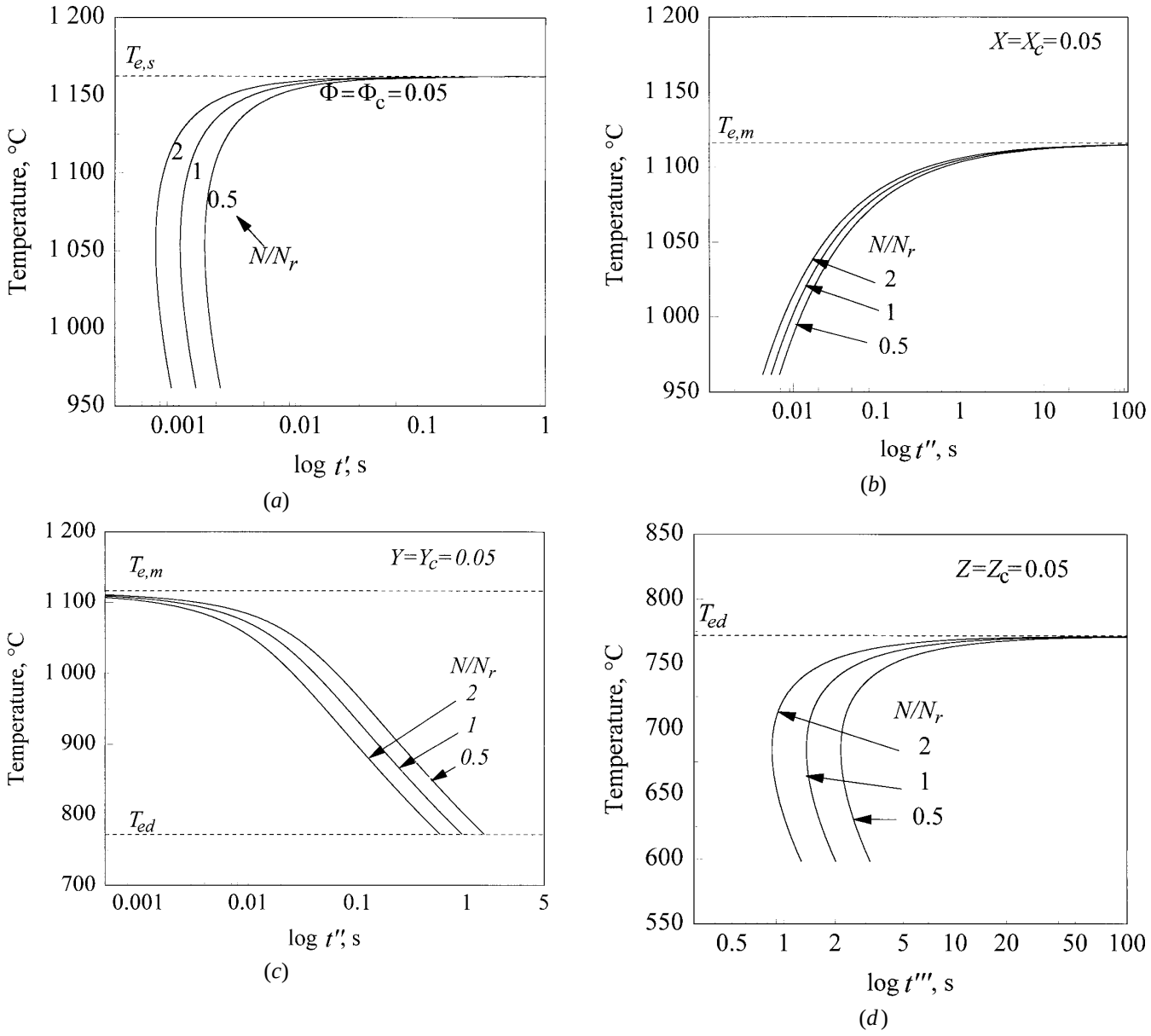

Fig. 9—Computed isothermal transformation diagrams for near-eutectic ductile cast iron. (*a*) The graphite/austenite eutectic transformation. (*b*) The ledeburite eutectic transformation ($f_{lb}^0 = 1$). (*c*) Graphite growth in austenite regime ($f_s = 1$). (*d*) The eutectoid transformation ($f_s = 1$, $Y = 1$). Input data as in Table III.

and diffusivity (D^γ or D^α) on the reaction kinetics. In contrast, the metastable eutectic transformation will only reveal a half C curve, because the growth rate here just depends on the bulk undercooling (Figure 9(b)). However, in both cases, a decrease in the N/N_r ratio will tend to shift the position of the transformation curves toward longer times in the diagrams as the spatial distance between graphite nodules increases. Moreover, a comparison with Figure 9(c) shows that the shape of the transformation curve for carbon diffusion in the austenite regime departs quite strongly from that observed for the other reactions. This is because the solubility of carbon in austenite decreases with temperature, which leads to a corresponding increase in the diffusion time when Y_c is fixed. Consequently, the situation described in Figure 9(c) is special in the sense that the transformation cannot be described by a unique C curve representing a constant fraction transformed.

D. *Volume Fractions of Constituent Phases*

Based on the response equations developed in the preceding sections, it is possible to construct a series of process diagrams, which display the contribution of each phase transformation to the total microstructure evolution. Examples of such diagrams are given in Figure 10. It is evident that the transformation behavior of ductile cast iron is complex and rather unpredictable in the sense that the microstructure evolution depends on the interplay between several reactions that are coupled. Each of these will have a profound effect

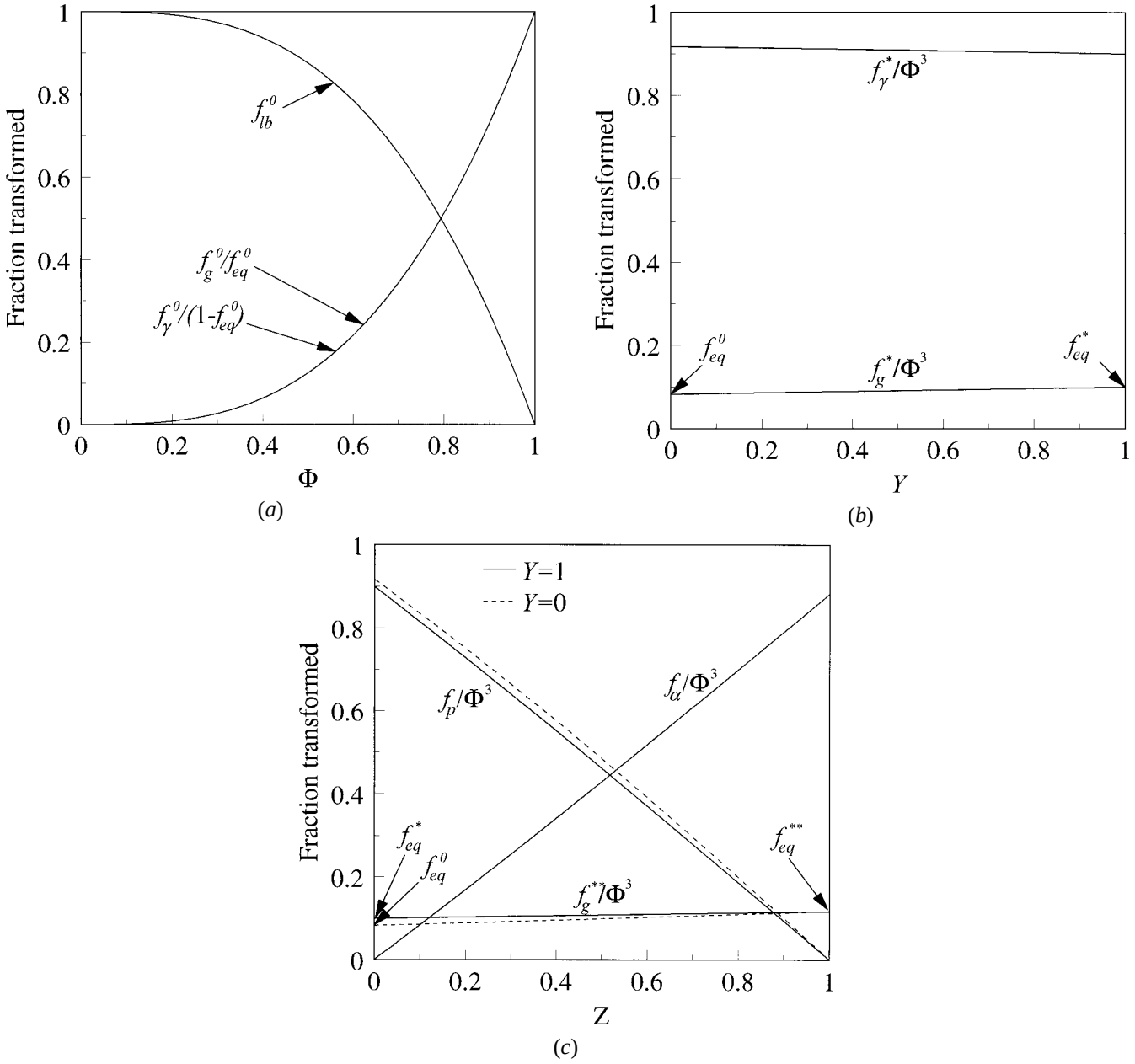

Fig. 10—Process diagrams for near-eutectic ductile cast iron showing the contribution of specific phase transformations to the total microstructure evolution. (*a*) The graphite/austenite eutectic transformation and the ledeburite eutectic transformation. (*b*) Carbon diffusion in the austenite regime. (*c*) The eutectoid transformation. Input data as in Table III.

on the final outcome, although the contribution from previous steps may be masked by subsequent transformations. Process diagrams of this kind are therefore useful, from both an academic and a practical point of view, because they provide the reader with an overall indication of the microstructural connections throughout the entire process route.

E. *Model Limitations*

In the derivation of the rate laws and the response equations, a number of simplifying assumptions have been made without any formal discussion. Some of these are rational in the sense that they are born out of well-accepted modeling principles, while others are less obvious and therefore more controversial. In the latter case, the justification relies solely on a good agreement between theory and experiments, and this matter will be fully addressed in Part II of the investigation.[20]

The key question is whether the present microstructure models also apply under thermal conditions that depart strongly from those experienced during directional solidification. The obvious answer to this is yes, as long as the microstructure evolution in a given position of the casting is only a function of the kinetic strength of the cooling cycle. In practice, the problem is more complicated due to segregation of alloying elements during solidification. Under such conditions, the transformation reactions become thermal path dependent, which means that the isokinetic concept

breaks down and should be replaced by the more general internal state variable approach. As shown in Appendix III, the effect of microsegregation can be easily incorporated in the process model without a significant increase in the computational effort, whereas inclusion of a macrosegregation model would require a full analysis of convective heat flow phenomena as well. A consideration of macrosegregation therefore is not possible within the framework of the present modeling approach.

V. CONCLUSIONS

In the present investigation, process modeling techniques have been applied to describe the multiple phase changes occurring during solidification and subsequent cooling of near-eutectic ductile cast iron, based on the internal state variable approach.

1. As a starting point, isothermal transformation behavior is first considered for the limiting case of early site saturation and steady-state 1-D diffusion-controlled growth. These solutions are later manipulated and rewritten in a differential form to cover nonisothermal microstructure evolution. The judicious construction of the constitutive equations makes full use of both dimensionless parameters and calibration techniques to eliminate poorly known kinetic constants. This is essential in order to reduce the total number of variables involved to an acceptable level.
2. In its simplest form, the microstructure evolution can be captured mathematically in terms of differential variation of two primary state variables with time for each of the relevant mechanisms. Since one of these represents the temperature, additional heat flow calculations or measured thermal data are required to solve the differential equations. In the latter case, the integration can be carried out using the more convenient isokinetic solutions, provided that the evolution equations are separable or can be made separable by a simple change of variables.
3. By considering the constraints provided by the phase diagram, a series of response equations has been developed to convert the current values of the state variables into equivalent volume fractions of constituent phases. These results may be conveniently presented in the form of a set of "master curves," which show the contribution from each transformation to the total microstructure evolution. Such process diagrams are useful, from both an academic and a practical point of view, because they provide the reader with an overall indication of the microstructural connections throughout the entire process route.

It is concluded that the combination of a microstructure model and a thermal model for heat flow calculations provides a powerful tool for alloy design and optimisation of cooling schedules for ductile cast iron, and an illustration of this is given in an accompanying paper (Part II).

ACKNOWLEDGMENTS

The authors acknowledge the financial support from Elkem as, Bjølvefossen ASA, Fesil AS, and the Norwegian Research Council.

APPENDIX I
Nomenclature

b	ratio between the thickness of the austenite and the graphite shells in a 3-D model
C	concentration (mol m^{-3})
pct C	carbon concentration in iron matrix (wt pct)
$C^{\alpha/\gamma}$	carbon concentration at α/γ interface (mol m^{-3})
$C^{\alpha/g}$	carbon concentration at α/g interface (mol m^{-3})
C^{g}	graphite concentration (mol m^{-3})
$C^{\gamma/\alpha}$	carbon concentration at γ/α interface (mol m^{-3})
$C^{\gamma/g}$	carbon concentration at γ/g interface (mol m^{-3})
$C^{\gamma/L}$	carbon concentration at γ/L interface (mol m^{-3})
$C^{L/\gamma}$	carbon concentration at L/γ interface (mol m^{-3})
C_m^{γ}	maximum carbon content in austenite (mol m^{-3})
C_{Si}^{0}	initial Si content in iron matrix (mol m^{-3})
C_{Si}^{L}	Si content in liquid iron (mol m^{-3})
d	inclusion diameter (m)
d_0	initial inclusion diameter (m)
dr_g	incremental value of r_g or Δr_g (m)
dr_α	incremental value of r_α (m)
dr_γ	incremental value of Δr_γ (m)
D^{α}	diffusion coefficient of carbon in ferrite ($m^2\ s^{-1}$)
D^{γ}	diffusion coefficient of carbon in austenite ($m^2\ s^{-1}$)
f	volume fraction of an arbitrary transformation product
f_{cf}	volume fraction of carbide/ferrite aggregates
f_g	volume fraction of graphite
f_g'	value of f_g before physical impingement of adjacent transformation volumes
f_{eq}	equilibrium volume fraction of graphite in the austenite regime
f_{eq}^{o}	value of f_{eq} at $T = T_{e,m}$
f_{eq}^{*}	value of f_{eq} at $T = T_{ed}$
f_{eq}^{**}	equilibrium volume fraction of graphite after the eutectoid transformation
f_g^{o}	volume fraction of graphite after solidification
f_g^{*}	volume fraction of graphite at the entry of the eutectoid transformation
f_g^{**}	volume fraction of graphite after completion of the eutectoid transformation
f_{lb}	volume fraction of ledeburite eutectic
f_{lb}'	value of f_{lb} before physical impingement of adjacent transformation volumes
f_{lb}^{o}	maximum volume fraction of ledeburite after solidification
f_{lb}^{*}	volume fraction of ledeburite at the entry of the eutectoid transformation
f_p	volume fraction of pearlite
f_α	volume fraction of ferrite
f_γ^{o}	volume fraction of austenite after solidification
f_γ^{*}	volume fraction of austenite at the entry of the eutectoid transformation
f_s	volume fraction of graphite/austenite eutectic
f_s'	value of f_s before physical impingement of adjacent transformation volumes
h_1, h_2	arbitrary functions of f, N, and T
k	partition coefficient in the segregation model
k_1	kinetic constant in the Wagner equation ($m^3\ s^{-1}$)
k_2	growth constant (m s^{-1} $°C^{-2}$)

K dimensionless concentration factor in the solid-state diffusion model
l position in bar referred to chilled end (m)
L latent heat of transformation (J m^{-3})
L_e latent heat released during the eutectoid transformation (J m^{-3})
L_m latent heat released during the ledeburite eutectic transformation (J m^{-3})
L_s latent heat released during the graphite/austenite eutectic transformation (J m^{-3})
M_1, M_2 temperature-dependent concentration factors in the solidification model
M_1^*, M_2^* temperature-dependent concentration factors in the solid-state diffusion model
M_3 temperature-dependent concentration factor in a 3-D solidification model
N number of particles (grains) per unit volume (no. m^{-3})
N_r number of particles (grains) per unit volume in reference alloy (no. m^{-3})
Q^α activation energy for diffusion of carbon in ferrite (kJ mol^{-1})
Q^γ activation energy for diffusion of carbon in austenite (kJ mol^{-1})
r radius (m)
r_g radius or width of the graphite layer (m)
r_g^o radius of graphite sphere after solidification (m)
r_{lb} radius of ledeburite eutectic nodule (m)
Δr_g increase in r_g due to solid-state diffusion (m)
Δr_α width of ferrite layer (m)
Δr_γ width of austenite layer (m)
R universal gas constant (8.314 J mol^{-1} K^{-1})
t time (s)
t' time referred to start of the graphite/austenite eutectic transformation (s)
t'' time referred to start of the ledeburite eutectic transformation (s)
t''' time referred to start of the eutectoid transformation (s)
t_1^* time constant in the kinetic model for the graphite/austenite eutectic transformation (s)
t_2^* time constant in the kinetic model for the ledeburite eutectic transformation (s)
t_3^* time constant in the kinetic model for graphite growth in the austenite regime (s)
t_4^* time constant in the kinetic model for the eutectoid transformation (s)
t_{ed} time for start of the eutectoid transformation (s)
$t_{n,s}$ time at which nucleation of graphite occurs (s)
$t_{n,m}$ time at which nucleation of ledeburite occurs (s)
t_{r_1} reference time in the kinetic model for the graphite/austenite eutectic transformation (s)
t_{r_2} reference time in the kinetic model for the ledeburite eutectic transformation (s)
t_{r_3} reference time in the kinetic model for graphite growth in the austenite regime (s)
t_{r_4} reference time in the kinetic model for the eutectoid transformation (s)
T temperature (°C or K)
T_i initial melt temperature (°C or K)
T_{ed} eutectoid temperature in the stable system (°C or K)
$T_{e,m}$ eutectic temperature in the metastable system (°C or K)
$T_{e,s}$ eutectic temperature in the stable system (°C or K)
$T_{n,s}$ graphite nucleation temperature (°C or K)
$T_{n,m}$ ledeburite nucleation temperature (°C or K)
T_r reference temperature (index refers to a specific transformation) (°C or K)
ΔT eutectic undercooling in stable system (°C or K)
ΔT_{r_1} value of ΔT at $T = T_{r_1}$ (°C or K)
ΔT^* eutectic undercooling in metastable system (°C or K)
$\Delta T_{r_2}^*$ value of ΔT^* at $T = T_{r_2}$ (°C or K)
ΔT^{**} eutectoid undercooling (°C or K)
$\Delta T_{r_4}^{**}$ value of ΔT^{**} at $T = T_{r_4}$ (°C or K)
v isothermal growth velocity of ledeburite nodules (m s^{-1})
V inclusion volume fraction (index r refers to reference alloy)
X linearized volume fraction of ledeburite
X' value of X before physical impingement of adjacent transformation volumes
X_c value of X at time $t'' = t_2^*$
X_r' value of X' at $T = T_{r_2}$
Y linearized volume fraction of graphite in austenite regime
Y' value of Y before physical impingement of adjacent transformation volumes
Y_c value of Y at time $t'' = t_3^*$
Y_r' value of Y' at $T = T_{r_3}$
Z linearized volume fraction of graphite in the two-phase $\alpha + \gamma$ regime
Z_c value of Z at time $t''' = t_4^*$
Φ linearized fraction of solid
Φ' value of Φ before physical impingement of adjacent transformation volumes
Φ_c value of Φ at time $t' = t_1^*$
Φ_r' value of Φ' at $T = T_{r_1}$
λ thermal conductivity (J s^{-1} m^{-1} K^{-1})
ρc volume heat capacity (J K^{-1} m^{-3})
ρ_g density of graphite (kg m^{-3})
ρ_{Fe} density of iron matrix (kg m^{-3})
Ω width of carbon diffusion zone (m)

APPENDIX II
Alternative derivation of constitutive equation for the graphite/austenite eutectic transformation

This treatment is based on the 3-D analytical solution of Su *et al.*[27] According to their model, the steady-state growth rate of the austenite shell is given by

$$\frac{dr_\gamma}{dt'} = D^\gamma \frac{r_g}{(r_\gamma - r_g) r_\gamma} \frac{(C^{\gamma/L} - C^{\gamma/g})}{(C^{L/\gamma} - C^{\gamma/L})} \qquad [A1]$$

Taking the ratio between the thickness of the austenite and graphite shells equal to b (with $b = 2.4$),[26] Eq. [A1] transforms to

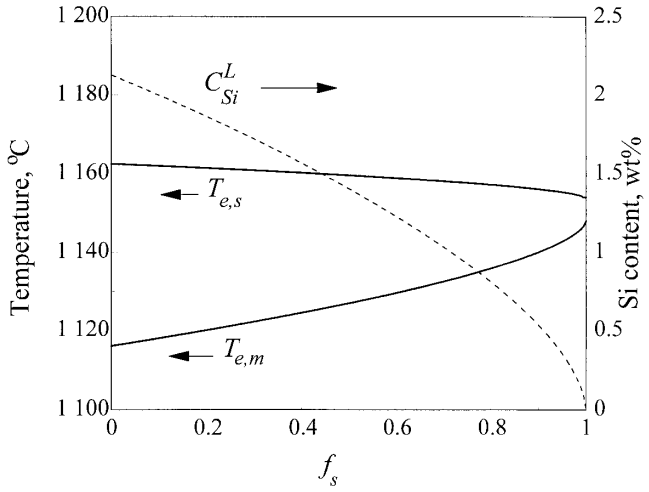

Fig. A1—Effect of Si depletion on the solidification behavior of an autonomous volume element in the casting. Input data as in Tables I and III.

$$\frac{dr_\gamma}{dt'} = D^\gamma \frac{1}{r_\gamma}(C^{\gamma/L} - C^{\gamma/g})M_3 \qquad [A2]$$

where M_3 is a temperature-dependent concentration factor, defined as

$$M_3 = \frac{1}{(C^{L/\gamma} - C^{\gamma/L})(b-1)} \qquad [A3]$$

Assuming isothermal conditions, integration of Eq. [A3] gives

$$r_\gamma = \sqrt{2M_3 D^\gamma (C^{\gamma/L} - C^{\gamma/g})(t')} \qquad [A4]$$

Besides the concentration factors M_1 and M_3, Eqs. [A4] and [12] are identical in the sense that they lead to the same expression for the time constant t_1^* in the Avrami equation.

APPENDIX III
Microsegregation model for Si

The microsegregation model outlined subsequently applies to an arbitrary volume element in the casting. In its simplest form, the Scheil equation for the liquid reads

$$C_{\mathrm{Si}}^L = C_{\mathrm{Si}}^o (1 - f_s)^{k-1} \qquad [A5]$$

where C_{Si}^o is the initial Si content in the iron, and k is the partition coefficient (the value of k is close to 1.6).

As solidification proceeds, the remaining iron melt becomes gradually depleted with respect to Si. This, in turn, leads to a shift in the equilibrium temperatures $T_{e,s}$ and $T_{e,m}$ for the stable and metastable eutectic transformation, as shown in Figure A1. It follows that the Si depletion will favor the formation of iron carbide during solidification, particularly at high cooling rates.

In the MATLAB* toolbox developed in Part II,[20] the microsegregation problem can be handled by defining the equilibrium temperatures $T_{e,s}$ and $T_{e,m}$ as global variables.

*MATLAB is a trademark of The Math Works Inc., Natick, MA.

REFERENCES

1. I. Minkoff: *The Physical Metallurgy of Cast Iron*, John Wiley & Sons Ltd., New York, NY, 1983.
2. R. Elliott: *Cast Iron Technology*, Butterworth and Co., London, 1988.
3. M. Rappaz: *Int. Mater. Rev.*, 1989, vol. 34, pp. 93-123.
4. D.M. Stefanescu: *Iron Steel Inst. Jpn. Int.*, 1995, vol. 35, pp. 637-50.
5. D. Venugopalan: *Metall. Trans. A*, 1990, vol. 21A, pp. 913-18.
6. A. Almansour, K. Matsugi, T. Hatayama, and O. Yanagisawa: *Mater. Trans., JIM*, 1996, vol. 37, pp. 612-19.
7. A. Almansour, K. Matsugi, T. Hatayama, and O. Yanagisawa: *Mater. Trans., JIM*, 1995, vol. 36, pp. 1487-95.
8. L. Nastac and D.M. Stefanescu: *AFS Trans.*, 1995, vol. 103, pp. 329-37.
9. R. Mai, B. Leube, and E. Schüle: *Giessereiforschung*, 1995, vol. 47, pp. 1-5.
10. Q. Chen, E.W. Langer, and P.N. Hansen: *Scand. J. Metall.*, 1995, vol. 24, pp. 48-62.
11. S. Chang, D. Shangguan, and D.M. Stefanescu: *Metall. Trans. A*, 1992, vol. 23A, pp. 1333-46.
12. E. Fras, W. Kapturkiewicz, and H.F. Lopez: *AFS Trans.*, 1992, vol. 100, pp. 583-91.
13. G. Upadhya, D.K. Banerjee, D.M. Stefanescu, and J.L. Hill: *AFS Trans.*, 1990, vol. 98, pp. 699-706.
14. M.F. Ashby: *Mater. Sci. Technol.*, 1992, vol. 8, pp. 102-11.
15. H.R. Shercliff, Ø. Grong, O.R. Myhr, and M.F. Ashby: *Proc. 3rd Int. Conf. On Aluminium Alloys (ICAA3)*, Trondheim, Norway, 1992, vol. III, Norwegian Institute of Technology, Trondheim, Norway, 1992, pp. 357-69.
16. H. Shercliff, P. Sargent, and R.L. Wood: *Modelling Materials Processing*, Cambridge University Engineering Department Technical Report CUED/C-MATS/TR206, Cambridge University, Cambridge, United Kingdom, 1993.
17. D.H. Bratland, Ø. Grong, H.R. Shercliff, O.M. Myhr, and S. Tjøtta: *Acta Mater.*, 1997, vol. 45, pp. 1-22.
18. Ø. Grong: *Metallurgical modelling of welding*, 2nd ed., The Institute of Materials, London, 1997.
19. O. Richmond: *Proc. Int. Conf. Aluminium Technology "89,"* The Institute of Materials, London, 1986, p. 615.
20. M.I. Onsøien, Ø. Grong, Ø. Gundersen, and T. Skaland: *Metall. Mater. Trans. A*, 1999, vol. 30A, pp. 1069-79.
21. J.W. Christian: *The Theory of Phase Transformations in Metals and Alloys—Part I*, Pergamon Press, Oxford, United Kingdom, 1975.
22. E. Scheil: *Arch. Eisenhüttenwes.*, 1934-35, vol. 8, pp. 565-71.
23. H.S. Carslaw and J.C. Jaeger: *Conduction of heat in solids*, 2nd ed., Oxford University Press, Oxford, United Kingdom, 1959.
24. T. Skaland, Ø. Grong, and T. Grong: *Metall. Trans. A*, 1993, vol. 24A, pp. 2321-45.
25. D.A. Porter and K.E. Easterling: *Phase Transformations in Metals and Alloys*, 2nd ed., Chapman & Hall, London, 1992.
26. S.E. Wetterfall, H. Fredriksson, and M. Hillert: *Journal Iron Steel Inst.*, 1972, vol. 210, pp. 323-33.
27. K.C. Su, I. Ohnaka, I. Yamauchi, and I. Fukusako: *Mater. Res. Symp.*, 1985, vol. 34, pp. 181-89.
28. M. Hillert: in *Recent Research on Cast Iron*, H.D. Merchant, ed., Gordon and Breach, New York, NY, 1969.
29. M.I. Onsøien, Ø. Grong, G. Rørvik, A. Nordmark, and T. Skaland: *Int. J. Cast Met. Res.*, 1997, vol. 10, pp. 17-26.
30. D.M. Stefanescu: *ASM Metals Handbook*, 9th ed., ASM INTERNATIONAL, Metals Park, OH, 1988, vol. 15, pp. 61-70.
31. C.J. Smithells: *Metals Reference Book*, 5th ed., Butterworth and Co., London, 1976.